

Deep Learning based Switching Filter for Impulsive Noise Removal in Color Images

Krystian Radlak, Lukasz Malinski, and Bogdan Smolka, *Member, IEEE*

Abstract—Noise reduction is one the most important and still active research topic in low-level image processing due to its high impact on object detection and scene understanding for computer vision systems. Recently, we can observe a substantial increase of interest in the application of deep learning algorithms in many computer vision problems due to its impressive capability of automatic feature extraction and classification. These methods have been also successfully applied in image denoising, significantly improving the performance, but most of the proposed approaches were designed for Gaussian noise suppression. In this paper, we present a switching filtering design intended for impulsive noise removal using deep learning. In the proposed method, the impulses are identified using a novel deep neural network architecture and noisy pixels are restored using the fast adaptive mean filter. The performed experiments show that the proposed approach is superior to the state-of-the-art filters designed for impulsive noise removal in digital color images.

Index Terms—deep learning, deep neural networks, image denoising, image enhancement, impulsive noise, switching filter

I. INTRODUCTION

IMAGE denoising is a long-standing research topic in low-level image processing that still receives much attention from computer vision community. Over the last three decades, a considerable increase in the effectiveness of algorithms took place but despite these improvements, modern miniaturized high-resolution, low-cost image sensors still provide a limited quality, when operating in low lighting conditions. Therefore, image enhancement and noise removal are very important operations of digital image processing.

In practice, we can observe various types of noise that significantly degrade the quality of captured images. One of them is the so-called *impulsive noise*, which may appear due to electric signal instabilities, corruptions in physical memory storage, random or systematic errors in data transmission, electromagnetic interferences, malfunctioning or aging camera sensors, and poor lighting conditions [1]–[5]. This type of noise causes a total loss of information at certain image locations because the original color channels information is replaced by random values.

In literature, impulse noise is typically classified into two main categories [6]–[8]. The first one is the Channel Together Random Impulse (CTRI), in which a pixel channel may be

replaced with any value in the image intensity range. The second noise model is Salt & Pepper Impulse Noise (SPIN), in which a corrupted pixel value is set to either the minimum or the maximum from a range of possible image values (so it is set to either 0 or 255 for an 8-bit image). In both models, the main parameter is the noise density ρ , which denotes the fraction of corrupted pixels in the processed image. In this paper, we focus on the CTRI model, which is more common and the proposed filter can be directly applied to the SPIN model.

The classical method for removal of impulsive noise is the median filter. Generally, the median concept for color images is based on vector ordering, in which image pixels are treated as three-dimensional vectors. This gives better results than processing image channels independently [9]–[11]. The basic example of filters utilizing the vector ordering concept is the Vector Median Filter (VMF) [12], which effectively removes the impulses, but fails when noise density is very high and impulses are grouped in clusters, which are retained forming colorful blotches.

Another drawback of filters based on vector ordering is the fact that every pixel of the image is processed, regardless of whether it is contaminated or not. This may result in strong signal degradation and introduces a visible blurring effect, especially in highly textured regions. In many applications, it may become an undesired property and therefore a plethora of improvements have been proposed in literature [1], [4], [13]–[17]. To preserve image details and still efficiently suppress impulsive noise, a family of filters based on fuzzy set theory was introduced, in which a combination of impulsive noise detection and a replacement scheme based on averaging is performed [18]–[23]. However, these methods still may alter clean pixels in the processed image.

An effective approach to retain uncorrupted pixels is based on the switching concept [24]. A general scheme of switching filter is presented in Fig. 1. In the majority of the switching techniques, it is necessary to determine the measure of dissimilarity between the processed color pixels and a threshold value that allows to classify the pixels as clean or distorted. One of the most popular measures of similarity used in switching filters is the ROAD (Rank-Ordered Absolute Differences) statistic introduced in [25], in which the trimmed cumulative distance of the pixels to their neighbors is utilized as a measure of pixel corruption.

Among switching filters, an important group of methods is based on the concept of a *peer group* [26]–[28], in which the membership of a central pixel of the filtering window to its local neighborhood is determined in terms of the number of

K. Radlak and Bogdan Smolka are with Faculty of Automatic Control, Electronics and Computer Science, Silesian University of Technology, Akademicka 16, 44100 Gliwice, Poland, e-mail: krystian.radlak@polsl.pl, bogdan.smolka@polsl.pl

Lukasz Malinski is with Faculty of Materials Engineering and Metallurgy, Silesian University of Technology, Krasinskiiego 8, 40-019 Katowice, Poland, e-mail: lukasz.malinski@polsl.pl

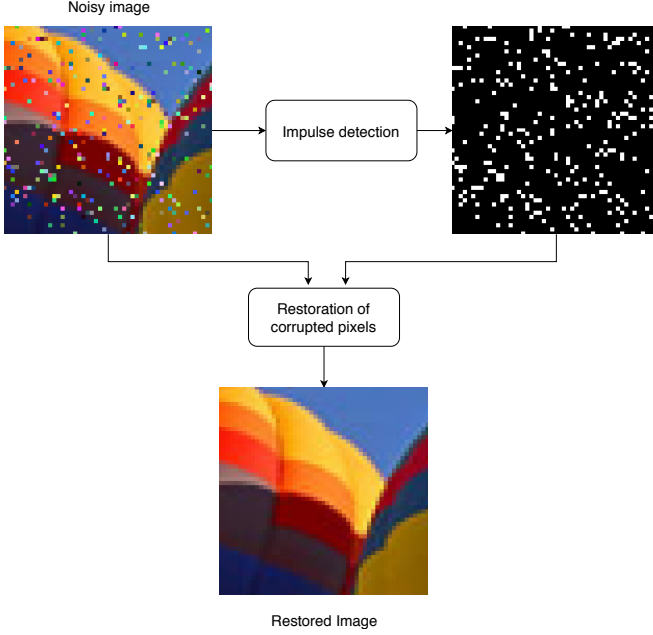


Fig. 1. A general scheme of a switching filter.

close pixels.

Another efficient family of switching filters utilizes the elements of quaternion theory [29]–[31]. In this concept, instead of the commonly used Euclidean distance in a chosen color space, the similarity between pixels is defined in the quaternion form.

Besides model-based methods, some switching filters also use classical machine learning approaches for impulses detection such as Support Vector Machines [32] and fully connected neural networks [33]–[36]. The detected impulses are restored using a median of uncorrupted pixels [33], [35], adaptive and iterative mean filters [34] or the edge-preserving regularization method [36].

Recently, thanks to easy access to large image datasets and advances in deep learning, the Convolutional Neural Networks (CNN) have led to a series of breakthroughs in various computer vision problems such as image segmentation, object recognition and detection. Concurrently, CNN have been also successfully applied for image denoising, focusing on the problem of Gaussian noise suppression. The recently proposed approaches significantly outperform classical model-based algorithms in terms of filtering efficiency and speed [37]–[39]. However, despite the fact that image denoising using deep learning for Gaussian noise removal has been well-studied, little work has been done in the area of impulsive noise removal [40]–[42].

In one of the most promising approaches, called Denoising Convolutional Neural Network (DnCNN), [43] the authors proved that residual learning and batch normalization are particularly beneficial in the case of Gaussian noise model. Unfortunately, the network based on residual learning formulation is not effective in the case of other types of operations like JPEG artifacts removal, deblurring or image resolution enhancement [44] and also in case of impulsive noise. Applying residual

learning for images contaminated by impulsive noise causes all pixels in the image to be altered, even those that were impulse-free, introducing unpleasant visual artifacts. Therefore, in this paper, we propose a modified version of the DnCNN called Impulse Detection Convolutional Neural Network (IDCNN).

In the proposed approach, in comparison to the basic DnCNN, we added a sigmoid layer to distinguish noise-free pixels from impulses and we reformulated the residual learning to the classification problem. In this way, the deep neural network is used as the impulse detector. Afterwards, the corrupted pixels are restored using an adaptive mean filter due to its good balance between simplicity and restoration effectiveness.

In summary, we make the following contributions:

- we propose a switching filter that uses deep learning for detection of corrupted pixels and adaptive mean filter for their restoration,
- we introduce a neural network architecture for impulse detection in images contaminated by impulsive noise,
- we analyze the impact of different network's parameters on impulse detection efficiency,
- we publish the source code of the proposed approach at <http://github.com/k-radlak/IDCNN>.

The paper is structured as follows. Section II describes the proposed switching filter based on deep learning, focusing on the architecture of the proposed IDCNN and its ablation study. Next Section presents a comparison of the proposed technique with state-of-the-art filters designed for impulsive noise removal. Finally, discussion and conclusions are given in Section IV.

II. IMPULSIVE NOISE DETECTION USING CONVOLUTIONAL NEURAL NETWORK

Recently, application of deep learning for image denoising received much attention from computer vision community due to its significant performance improvement in comparison to the classical machine learning algorithms. One of the most interesting methods, inspired by VGG network [45], intended for Gaussian noise is the Denoising Convolutional Neural Network (DnCNN) introduced by Zhang et al. [43].

The DnCNN contains a sequence of convolutional layers followed by Rectified Linear Unit (ReLU) [46] and Batch Normalization (BN) [47]. The first layer has a convolution filter and ReLU activation. The second and each consecutive layer consists of a convolution filter, BN and ReLU activation, except the last layer which uses only convolution. The training of the network is based on the concept of deep residual learning [48], in which the network does not estimate the original values of the undistorted image, but instead learns to estimate the difference between noisy and clean image.

More formally, let us assume that Y denotes a noisy image that is an input of DnCNN, X stands for a clean image and $\mathcal{R}(Y)$ is the output of the network, where $Y = X + \mathcal{R}(Y)$. The estimation of X can be formulated as $\hat{X} = Y - \mathcal{R}(Y)$.

The DnCNN filter outperforms most of the state-of-the-art algorithms designed for Gaussian noise removal, but due to the fact that it uses residual learning, the original DnCNN trained

on impulsive noise model also alter non-corrupted pixels as was shown in [42]. Therefore, in the proposed approach, we modified the original DnCNN architecture to ensure that noise-free pixels will be not affected and we introduced IDCNN.

In the proposed IDCNN, instead of the usage of residual learning, we employed all layers proposed in DnCNN for feature extraction and we added a sigmoid layer which estimates the probability of the pixel being an impulse or noise-free. The architecture of the proposed network is depicted in Fig. 2.

The introduced architecture also required a change in the training procedure. In the original DnCNN, during training the images are divided into a small square and non-overlapping patches of size $p \times p$. The loss function is then calculated between clean patches and the denoised one. In our approach, we generate a ground truth noise map M and in the training procedure we calculate the loss function between patches cropped from M and the noise map \hat{M} , estimated by the network as shown in Fig. 3. More formally, the loss function is defined as follows:

$$L(\Theta) = \frac{1}{N} \sum_{i=1}^N (M_i - \hat{M}_i)^2, \quad (1)$$

where Θ denotes a set of trainable parameters, M_i, \hat{M}_i denote for each patch i the original and the estimated noise map respectively, and N denotes the number of patches (small cropped images) used in the training. Finally, the output of the IDCNN is a probability map that has to be binarized using a threshold to finally classify a pixel as either noisy or undistorted.

In order to restore the detected noisy pixels, we used the modified version of the adaptive arithmetic mean filter introduced in [34], in which the authors proved that this approach gives satisfying image quality and reasonable computational speed. This algorithm of restoration of the detected noisy pixel can be summarized as follows:

- 1) Select initial window of size $W = 3 \times 3$ centered at the detected noisy pixel that should be replaced and calculate the number of pixels that are not corrupted by noise (using using an appropriate detection detector). If the number of uncorrupted pixels is lower than 1 then go to step 2 else go to step 4.
- 2) Increase the size of W by 2.
- 3) Calculate the number of uncorrupted pixels inside W and if the number of uncorrupted pixels is lower than 1 then go to step 2 else go to step 4.
- 4) Replace the current pixel by the average of all uncorrupted pixels inside W .

The proposed algorithm should be applied to restore all pixels that were classified by the network as impulses. However, it is worth mentioning here that the corrupted pixels can be replaced using other more robust techniques, e.g. image restoration algorithm based on deep neural network introduced in [49]. This issue will be the subject of follow-up research.

A. Ablation study

In order to evaluate the performance of the proposed network, we performed several experiments. We started with the

TABLE I
SUMMARY OF THE NETWORK PARAMETERS.

Parameter	Value
Number of convolutional layers	17
Number of filters in convolutional layer	64
Size of convolutional window	3×3
Number of epochs	50
Learning rate	0.001
Learning rate decay	0.1
Epoch in which learning rate decay is used	30
Batch size	128
Weights initialization	Glorot uniform initializer [50]
Weights optimization	ADAM optimizer [51]
Patch size in the training	41×41

default parameters that were proposed for DnCNN [43]. These parameters are summarized in Tab. I.

Additionally, for training purposes, all images were resized using bicubic interpolation in four scales $\{1, 0.9, 0.8, 0.7\}$ and we applied simple data augmentation: image rotations (90° , 180° , 270°) and image flipping in the up-down direction. Here it is worth mentioning that small patches were used only in the training phase, but in inference, the obtained convolution masks were applied to the whole image at once.

In our experiments, similarly to the authors of the DnCNN approach, we used Berkeley segmentation dataset (BSD500) [52] that consists of 500 natural images in resolution 481×321 . Example images from BSD500 are depicted in Fig. 4. For testing purposes, we used dataset introduced in [28] consisting of 100 color images in resolution 640×480 , which are presented in Fig. 5. In this paper, all presented results were obtained on this dataset.

For training purposes, these images were contaminated using the CTRI model. In this model each pixel $\mathbf{x}_i \in X, i = 1, 2, \dots, Q$ is contaminated with probability ρ and each channel obtains a new value $v_q, q = 1, 2, 3$ from the range $[0, 255]$ and drawn from a uniform distribution. This model can be formally defined as

$$\mathbf{y}_i = \begin{cases} (v_1, v_2, v_3) & \text{with probability } \rho, \\ \mathbf{x}_i & \text{with probability } 1 - \rho, \end{cases} \quad (2)$$

where \mathbf{y}_i denotes a noisy image pixel.

In order to evaluate the noise detection efficiency of the proposed network and impact of the network's parameters, we propose to transform the problem into classification domain, instead of using traditional measures for image denoising. In the proposed evaluation methodology, the result of noise detection is represented by the estimated noise map \hat{M} and is compared to the ground truth map M . Then, impulsive noise detection problem can be transformed into noisy vs. clean pixels classification and the results can be presented using a confusion matrix that reports the number of True Positives (TP), True Negatives (TN), False Positives (FP), False Negatives (FN). For the impulse detection problem

- TP are pixels that were correctly recognized as impulses,
- TN are pixels that were correctly recognized as not being contaminated,
- FP are pixels that were incorrectly classified as noisy,

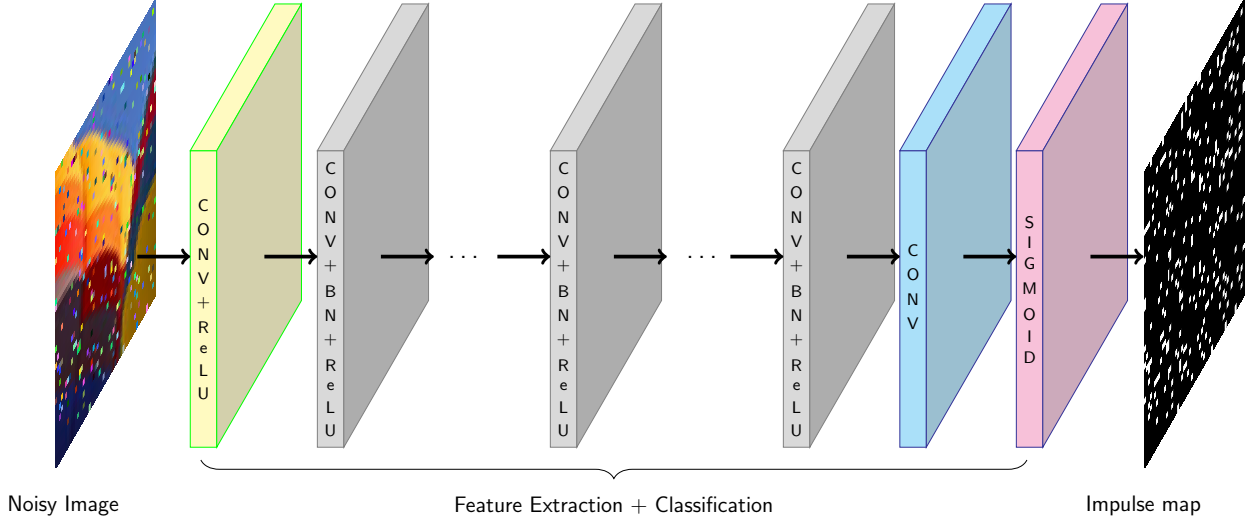


Fig. 2. The architecture of the proposed network for impulsive noise detection.

- FN are pixels that were incorrectly classified as uncorrupted.

Finally, the network performance can be evaluated using weighted accuracy (wACC) defined as

$$\text{wACC} = \rho \frac{\text{TP}}{\text{TP} + \text{FN}} + (1 - \rho) \frac{\text{TN}}{\text{TN} + \text{FP}}.$$

Weighted accuracy summarizes how many pixels were correctly classified when the classes are unbalanced and their cardinalities depends on selected noise intensity γ , but this metric does not distinguish what type of errors we made if we miss an impulse or incorrectly classify a clean pixel as noisy.

In statistical hypothesis testing, two types of errors are defined. Type I error occurs when a true null hypothesis is incorrectly rejected and it is also known as False Positive. A type II error occurs when the null hypothesis is false, but erroneously fails to be rejected and it is known as False Negative. Therefore in this work, we used two additional metrics that allow evaluating the portion of both types of errors that are made by the proposed detector. First of them is the False Positive Rate (FPR) defined as

$$\text{FPR} = \frac{\text{FP}}{\text{FP} + \text{TN}},$$

which shows the ratio of incorrectly classified clean pixels as impulses to the total number of clean pixels in the processed image. The second of them is the False Negative Rate (FNR) defined as

$$\text{FNR} = \frac{\text{FN}}{\text{TP} + \text{FN}},$$

which shows the ratio of incorrectly detected noisy pixels to the total number of impulses in an image. To evaluate the network performance on the whole test set, we determined wACC, TPR and FPR for each image and the average for all images from the test set was calculated.

To correctly localize impulses in the image based on the output of the proposed IDCNN, in the first step it is necessary

to estimate the proper value of the threshold to select, which pixels are contaminated by impulsive noise. Selection of the optimal threshold typically can significantly affect the final results, but we noticed that the values of the probabilities returned by the network are close to 0 if a pixel is clean and close to 1 if a pixel is classified as an impulse. Example histograms with distributions of probabilities that a pixel is an impulse returned by IDCNN are presented in Fig. 6 (on the left we present only a selected part of the histogram and the plot, on the right we show parts of the same histogram but with a different range on the x-axis). Therefore, in our research, we set the probability threshold to 0.5 as it does not have any impact on the classification results.

In order to better understand the influence of different parameters on the final performance of the proposed network, we conducted some additional experiments. In the first one, we check whether the network impulse detection efficiency is repeatable when we start the training procedure from scratch. The changes of the average wACC, FPR, and FNR calculated on test dataset during the training are presented in Fig. 7 and in Tab. II.

As can be observed, the results are repeatable and independent from the experiment repetition and the networks start to stabilize and converge to its final performance when the learning rate is decreased after 30 epochs. Additionally, we can see that the average FPR is relatively low and wACC quite well reflects the network performance. Therefore, in the rest of the paper, we present the wACC metric only.

In the next experiment, we evaluated the influence of the patch size p used in the training procedure on the final average performance of the network (see Fig. 8 and Tab III). We evaluated our method using the following patch sizes: $\{9, 11, 21, 31, 41, 51, 61, 71\}$. For smaller patch sizes, the network was not able to learn and therefore the results are not shown.

As can be observed, if the patch size used in the training

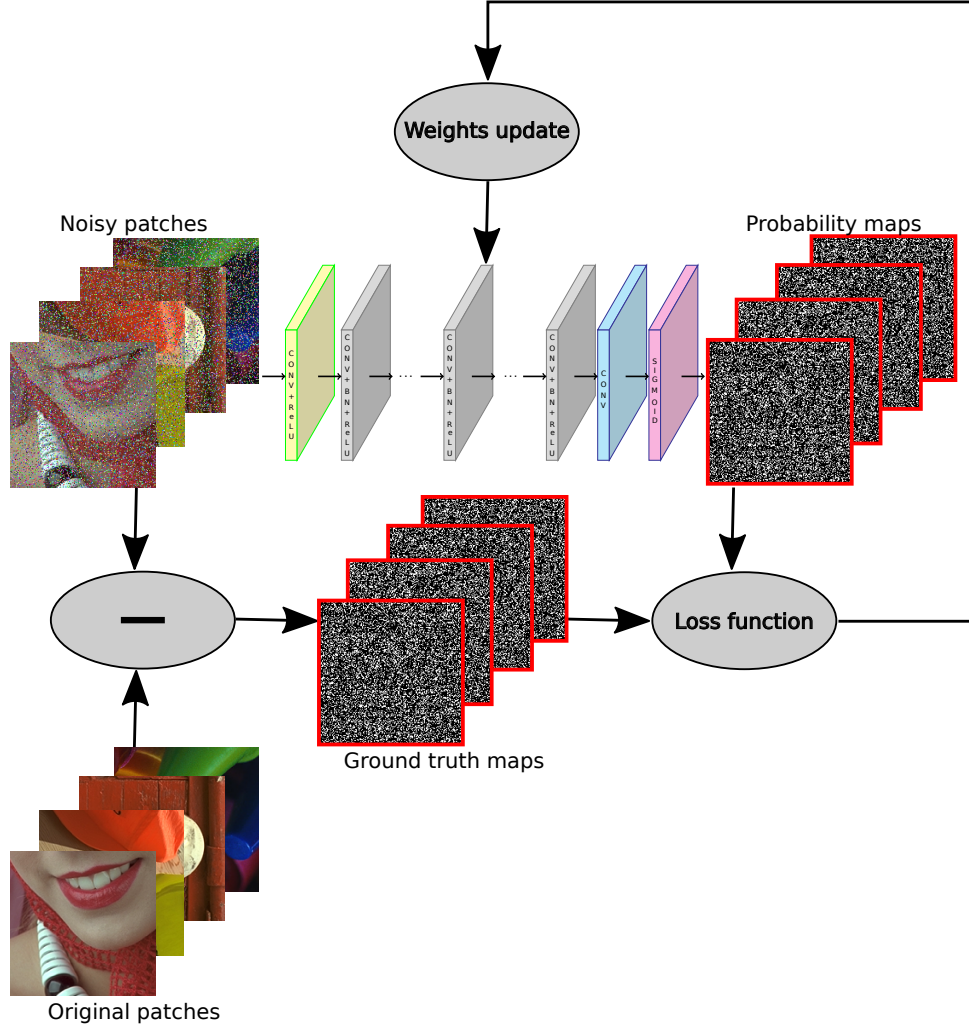


Fig. 3. Training of the proposed IDCNN detector.

is greater than or equal to 21×21 , the optimal performance of the network is obtained. However, the increase of the patch size does not boost the network's performance, but it makes training more time consuming, because the loss function is calculated between bigger patches. Therefore, the selected patch size cannot be too small nor too big it would only increase the training time.

In the next experiment, we analyzed the impact of the type of dataset used in training procedure and its size on the final network performance. We selected two additional datasets: the PASCAL VOC2007 dataset [53] and the Google Open Images Dataset V4 (GoogleV4) [54] introduced for object detection purposes. Both datasets contain high quality images and we selected randomly 500 pictures. The PASCAL VOC2007 dataset consists of images which present 20 classes of various objects. The GoogleV4 dataset contains images, which cover 600 classes, but in our research we selected only 50 classes. Therefore both datasets consist of limited texture examples (e.g. images that depict only trains) since the content of the used test dataset is much wider. Additionally, for GoogleV4 dataset we also decreased the original resolution four times to ensure similar resolution in all training and test

datasets. Example images from both datasets are presented in Figs. 9 and 10.

The influence of the size of the training dataset on the final average performance of the network is shown in Fig. 11 and summarized in Tab. IV. As can be observed, if the size of the dataset is increased, then the average wACC is also growing. The highest average wACC was achieved for GoogleV4 dataset, but the difference between various datasets is rather small. The performed experiment also shows that the training of the network requires sufficient amount of data in the training process to achieve expected effectiveness. However, the optimal performance can be achieved on different datasets. Additionally, we can notice that when the noise density increases, the network needs more data in the training. Finally, we recommend to use 500 images in the training, which are divided into small patches in the training, but we need to remember that the final number of patches can differ depending on image resolution. In one our experiment, the total number of non-overlapping patches of size 41×41 generated for BSD500 dataset was equal to 120500.

The last issue that we would like to address in the scope of this work was what noise density level should be used in



Fig. 4. Example images from Berkeley segmentation dataset (BSD500) [52].

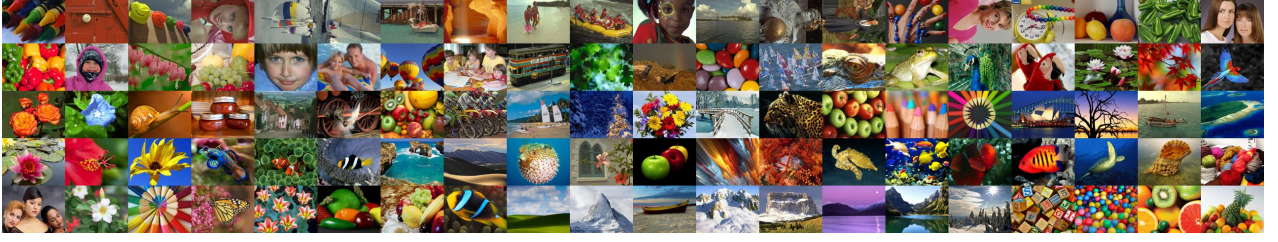


Fig. 5. Test dataset made available by Malinski and Smolka [28].

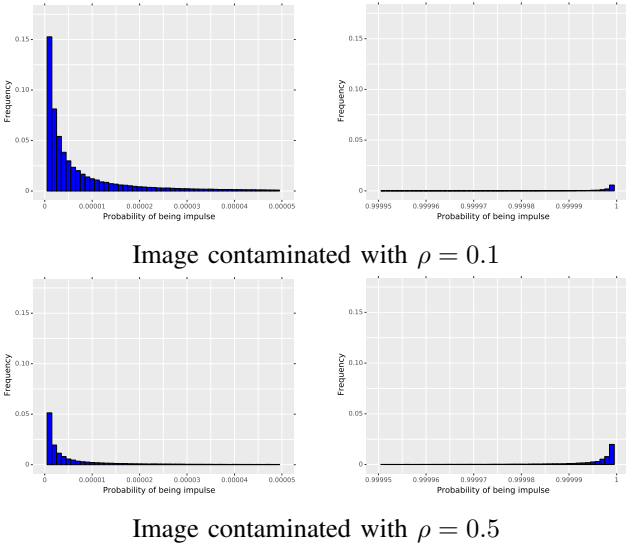


Fig. 6. Noise probability map distributions estimated by the proposed IDCNN for the example image.

the training procedure to obtain optimal network performance. For the original DnCNN, the authors proved that it was not so important what intensity level of Gaussian noise was used in the training and the network trained with $\sigma = 25$ was able to denoise images corrupted with different noise density. To confirm this behavior for impulsive noise, we trained the network with patches contaminated with noise density $\rho = \{0.1, 0.3, 0.5\}$. Additionally, we trained the network with patches contaminated with randomly selected noise probability from the range $[0.1, 0.5]$. This experiment is denoted in this paper as random and the results are depicted in Fig 12 and

TABLE II
REPEATABILITY OF THE TRAINING PROCEDURE ON BSD500 DATASET.

ρ	Training repetition				
	Average wACC				
	1	2	3	4	5
0.1	0.9985	0.9987	0.9987	0.9985	0.9987
0.2	0.9984	0.9986	0.9986	0.9985	0.9985
0.3	0.9980	0.9981	0.9982	0.9981	0.9980
0.4	0.9970	0.9971	0.9972	0.9970	0.9970
0.5	0.9945	0.9944	0.9944	0.9941	0.9944
ρ	Average FPR				
	1	2	3	4	5
	1	2	3	4	5
0.1	0.0014	0.0013	0.0013	0.0015	0.0012
0.2	0.0014	0.0012	0.0012	0.0014	0.0013
0.3	0.0014	0.0012	0.0012	0.0013	0.0013
0.4	0.0017	0.0014	0.0014	0.0013	0.0015
0.5	0.0020	0.0018	0.0016	0.0015	0.0018
ρ	Average FNR				
	1	2	3	4	5
	1	2	3	4	5
0.1	0.0018	0.0016	0.0015	0.0015	0.0018
0.2	0.0025	0.0023	0.0022	0.0023	0.0024
0.3	0.0035	0.0034	0.0033	0.0034	0.0034
0.4	0.0051	0.0052	0.0050	0.0054	0.0051
0.5	0.0090	0.0093	0.0095	0.0103	0.0094

summarized in Tab. V.

As can be observed, the highest values are observed if the noise level during training and during tests was the same. In case of using a random noise density during training, the results are very close to the optimal performance. The highest deviations from the optimal average wACC were obtained if the patches were contaminated with low noise density level during training and heavy noise at testing phase and vice versa.

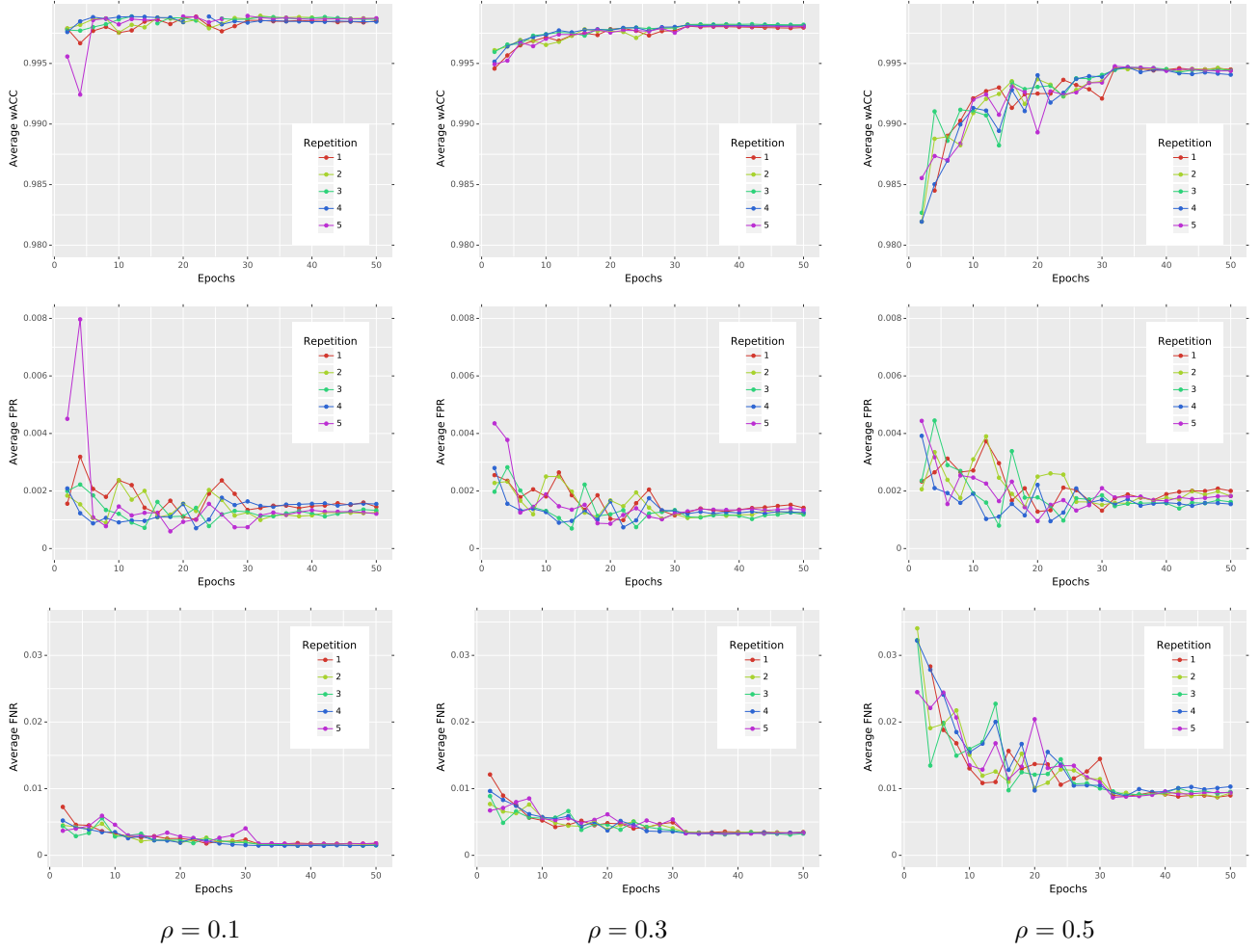


Fig. 7. Repeatability of the training procedure on BSD500 dataset.

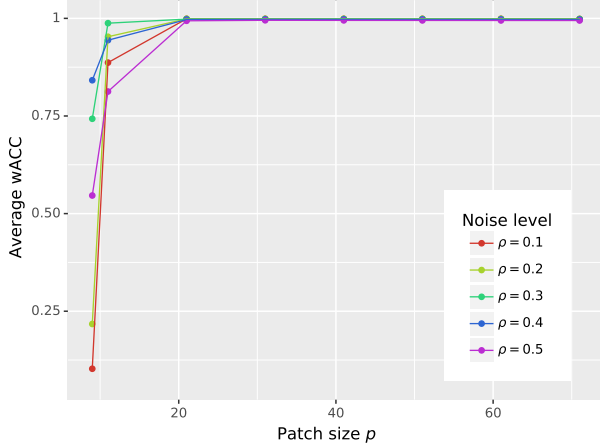


Fig. 8. Impact of the patch size used in the training procedure on final detection weighted accuracy of the network.

In most cases, the optimal wACC was obtained using $\rho = 0.3$ and for other noise levels in the test phase, the performance was very close to the optimal, therefore we recommend to use this value during training.

TABLE III
IMPACT OF THE PATCH SIZE USED IN THE TRAINING PROCEDURE ON FINAL DETECTION PERFORMANCE OF THE NETWORK.

ρ	Average wACC						
	Patch size p						
	9	11	21	31	41	51	61
0.1	0.1005	0.1026	0.9987	0.9986	0.9987	0.9985	0.9988
0.2	0.2063	0.2159	0.9985	0.9985	0.9985	0.9985	0.9986
0.3	0.5258	0.5887	0.9980	0.9980	0.9981	0.9980	0.9980
0.4	0.6003	0.6107	0.9969	0.9972	0.9971	0.9970	0.9969
0.5	0.5000	0.5005	0.9938	0.9950	0.9946	0.9944	0.9942

To summarize, the performed experiments confirmed that the analyzed parameters proposed for DnCNN can be used as a default for the proposed IDCNN. However, it will be indispensable in the future to more carefully analyze the impact of the diversity of the dataset used during training on the final performance of the network.

III. COMPARISON WITH THE STATE-OF-THE-ART DENOISING METHODS

The proposed switching filter that can be regarded as an extension of the DnCNN to detect impulses in the image with

[illegible]

In this work, the following state-of-the-art filters were taken for comparison: Denoising Convolutional Neural Network trained on impulsive noise (DnCNN) [42], Fast Averaging

TABLE IV
IMPACT OF THE TYPE OF DATASET USED IN THE TRAINING AND ITS SIZE
ON THE AVERAGE wACC OF THE NETWORK.

Average wACC							
BSD500							
Dataset size							
ρ	10	50	100	200	300	400	500
0.1	0.9910	0.9969	0.9983	0.9982	0.9985	0.9985	0.9987
0.2	0.9889	0.9962	0.9979	0.9982	0.9983	0.9984	0.9986
0.3	0.9830	0.9946	0.9970	0.9976	0.9978	0.9980	0.9982
0.4	0.9701	0.9909	0.9952	0.9962	0.9967	0.9970	0.9972
0.5	0.9434	0.9807	0.9898	0.9924	0.9938	0.9945	0.9944
VOC2007							
Dataset size							
ρ	10	50	100	200	300	400	500
0.1	0.9906	0.9985	0.9985	0.9992	0.9993	0.9991	0.9992
0.2	0.9872	0.9977	0.9985	0.9989	0.9990	0.9990	0.9990
0.3	0.9798	0.9962	0.9977	0.9982	0.9984	0.9985	0.9986
0.4	0.9647	0.9931	0.9958	0.9967	0.9972	0.9973	0.9974
0.5	0.9345	0.9849	0.9894	0.9922	0.9930	0.9926	0.9939
GoogleV4 dataset							
Dataset size							
ρ	10	50	100	200	300	400	500
0.1	0.9907	0.9980	0.9983	0.9990	0.9986	0.9990	0.9993
0.2	0.9850	0.9979	0.9983	0.9988	0.9987	0.9990	0.9991
0.3	0.9766	0.9973	0.9979	0.9985	0.9985	0.9987	0.9988
0.4	0.9614	0.9954	0.9964	0.9975	0.9975	0.9980	0.9981
0.5	0.9332	0.9886	0.9900	0.9932	0.9937	0.9950	0.9952

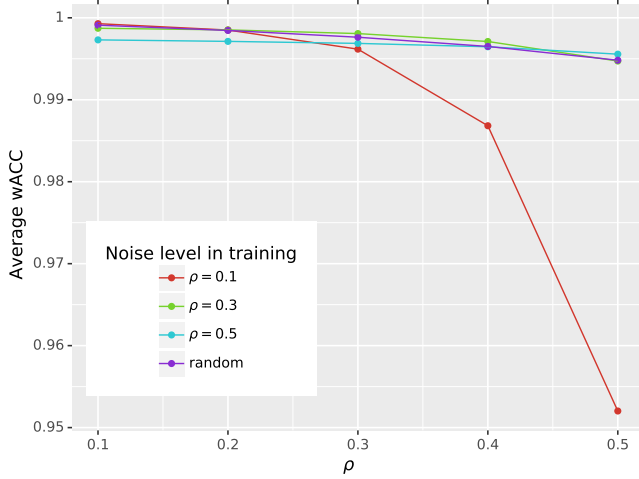


Fig. 12. Impact of the noise density used during training on the final network performance and its ability to detect impulses in test images contaminated with different noise density.

Peer Group Filter (FAPGF) [28], Fast Adaptive Switching Trimmed Arithmetic Mean Filter (FASTAMF) [24], Fast Fuzzy Noise Reduction Filter (FFNRF) [21], Fuzzy Rank-Ordered Differences Filter (FRF) [56], Impulse Noise Reduction Filter (INRF) [57], Patch-based Approach for the Restoration of Images affected by Gaussian and Impulse noise (PARIGI) [58], Peer Group Filter (PGF) [27]. As our final method in evaluation, we used two switching filters. Both methods of impulse detection used proposed IDCNN, but the final networks were trained on two different datasets: BSD500 (IDCNN_{BSD500}) and GoogleV4 (IDCNN_{Google}).

TABLE V
IMPACT OF THE NOISE DENSITY USED DURING TRAINING ON THE FINAL
NETWORK PERFORMANCE AND ITS ABILITY TO DETECT IMPULSES IN
TEST IMAGES CONTAMINATED WITH DIFFERENT NOISE DENSITY.

Average wACC				
Noise density in the training				
ρ	random	0.1	0.3	0.5
0.1	0.9991	0.9993	0.9987	0.9973
0.2	0.9985	0.9985	0.9985	0.9971
0.3	0.9976	0.9962	0.9981	0.9969
0.4	0.9965	0.9868	0.9971	0.9965
0.5	0.9948	0.9520	0.9947	0.9956

The numerical results are shown in Table VI using four representative test images chosen from the test dataset [28], which are presented in Fig. 13. As can be observed, in all cases, the results of the proposed switching filter that uses IDCNN for impulse detection and adaptive mean filter for image restoration outperform other state-of-the-art techniques.

The visual comparison of the obtained results is depicted in Fig. 15. As can be observed, the proposed IDCNN is able to correctly localize almost all impulses and the visible artifacts are the effect of insufficient quality of restoration of detected impulses. Therefore, future work will be focused on the improvement of the efficiency of the noisy pixel replacement method.

To confirm that the main source of error is the method of interpolation, we presented the Aim Diagram (AD) which separates the distribution of errors that was caused by improper classification of the impulses. Using traditional metrics, we are not able to evaluate whether the main source of the error was caused by incorrect impulse detection or corrupted pixels restoration. In the proposed diagrams, the radiuses in the circle denote the proportion of the MAE metric calculated independently for pixels that are TP, FP and FN respectively. The error for TN pixels is equal to zero and therefore this radius is not presented on the plots. The AD calculated for MAE metric is presented in Fig. 16. As can be observed, the proposed impulse detector CNN_{BSD500} and CNN_{GoogleV4}, trained on BSD500 and GoogleV4 datasets respectively, almost perfectly detected all impulses and the main contribution to the MAE error comes from insufficient quality of detected impulse restoration. It shows that in further research the quality of the proposed filter could be improved if we would use a better noisy pixel interpolation method.

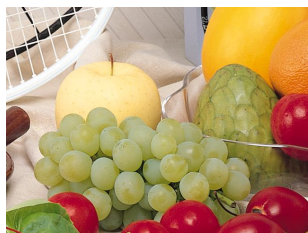
Finally, the average values of selected metrics calculated on the test dataset [28] are presented in Tab. VII. We also included the representative boxplots for PSNR measure to show the distribution of the obtained results (see Fig. 14). As can be observed, the average results of the proposed filter based on deep learning are significantly better than state-of-the-arts filters in terms of all used metrics. Additionally, the proposed switching filter allows achieving much better results than original DnCNN trained for impulsive noise.

TABLE VI
COMPARISON OF THE DENOISING EFFICIENCY OF THE PROPOSED NETWORK FOR IMPULSIVE NOISE REMOVAL WITH THE STATE-OF-THE-ART METHODS
ON SELECTED REPRESENTATIVE IMAGES FROM TEST DATASET [28].

ρ	IDCNN _{BSD500}	IDCNN _{GoogleV4}	DnCNN	FAPGF	FASTAMF	FFNRF	FRF	INRF	PARIGI	PGF
FRUITS										
PSNR [dB]										
0.1	39.78	40.35	35.18	37.61	38.30	36.97	36.03	33.90	34.66	37.03
0.2	36.54	37.24	36.47	34.69	35.47	33.20	33.21	32.03	33.14	32.52
0.3	34.22	35.00	33.75	32.19	32.70	28.44	30.80	30.28	31.00	27.85
0.4	32.37	33.20	31.37	29.89	29.86	23.95	27.62	28.43	29.25	23.52
0.5	29.71	30.08	27.87	26.53	25.40	19.88	22.27	25.26	26.81	19.67
MAE										
0.1	0.45	0.42	1.27	0.55	0.50	0.51	0.55	0.84	1.51	0.53
0.2	0.88	0.84	1.66	1.07	0.96	1.08	1.07	1.41	1.93	1.21
0.3	1.36	1.30	2.31	1.73	1.52	2.12	1.72	2.14	2.51	2.40
0.4	1.90	1.81	3.25	2.61	2.30	4.16	2.72	3.14	3.10	4.69
0.5	2.70	2.65	5.03	4.20	4.07	8.26	5.53	4.99	3.93	9.21
SSIM										
0.1	0.985	0.987	0.972	0.979	0.983	0.978	0.978	0.973	0.935	0.974
0.2	0.970	0.974	0.953	0.956	0.966	0.940	0.958	0.947	0.918	0.927
0.3	0.950	0.958	0.920	0.921	0.941	0.842	0.934	0.909	0.896	0.824
0.4	0.925	0.936	0.861	0.861	0.893	0.649	0.877	0.843	0.872	0.640
0.5	0.880	0.886	0.744	0.746	0.772	0.420	0.660	0.721	0.842	0.433
BALLOONS										
PSNR [dB]										
0.1	40.09	40.91	36.65	36.94	38.18	37.09	36.26	34.52	36.15	37.27
0.2	36.83	37.75	34.52	34.56	35.54	33.35	33.16	32.84	34.74	32.59
0.3	34.17	35.13	32.22	32.24	32.94	28.37	30.54	31.02	32.24	27.53
0.4	31.90	33.30	30.03	29.90	30.04	23.52	27.29	28.75	30.13	22.90
0.5	28.56	29.85	26.78	26.25	25.11	19.20	21.89	25.14	28.31	18.85
MAE										
0.1	0.31	0.29	1.18	0.45	0.37	0.35	0.41	0.67	0.81	0.38
0.2	0.61	0.58	1.66	0.83	0.70	0.77	0.82	1.05	1.09	0.88
0.3	0.97	0.91	2.31	1.37	1.11	1.65	1.36	1.62	1.53	1.98
0.4	1.40	1.26	3.30	2.14	1.71	3.71	2.23	2.46	1.99	4.43
0.5	2.26	1.99	5.39	3.77	3.49	8.29	4.88	4.34	2.58	9.69
SSIM										
0.1	0.993	0.994	0.978	0.983	0.989	0.987	0.985	0.982	0.976	0.980
0.2	0.985	0.986	0.960	0.963	0.977	0.955	0.969	0.964	0.969	0.939
0.3	0.973	0.977	0.926	0.929	0.960	0.851	0.948	0.932	0.955	0.823
0.4	0.954	0.966	0.852	0.863	0.920	0.635	0.900	0.867	0.941	0.612
0.5	0.902	0.923	0.690	0.724	0.783	0.378	0.690	0.725	0.920	0.375
PEPPERS										
PSNR [dB]										
0.1	47.75	47.88	40.50	44.52	45.88	43.33	44.09	40.83	39.72	41.21
0.2	43.85	44.41	36.92	40.54	41.34	35.52	39.99	37.86	38.43	33.44
0.3	40.67	41.64	33.99	35.93	36.50	28.11	36.12	34.39	36.68	26.48
0.4	37.54	39.16	30.51	31.98	31.75	22.28	29.99	30.60	34.71	21.09
0.5	32.38	34.02	26.51	26.79	24.67	17.59	22.17	24.64	31.62	16.91
MAE										
0.1	0.17	0.17	1.16	0.21	0.18	0.23	0.22	0.36	0.51	0.27
0.2	0.36	0.35	1.75	0.47	0.40	0.62	0.49	0.72	0.79	0.77
0.3	0.59	0.57	2.53	0.92	0.72	1.63	0.87	1.27	1.13	2.19
0.4	0.89	0.83	3.82	1.66	1.27	4.30	1.62	2.14	1.52	5.86
0.5	1.52	1.34	6.25	3.37	3.36	10.54	4.45	4.41	2.13	13.58
SSIM										
0.1	0.997	0.997	0.952	0.992	0.995	0.993	0.993	0.991	0.983	0.987
0.2	0.993	0.994	0.905	0.979	0.989	0.960	0.986	0.977	0.977	0.938
0.3	0.988	0.990	0.850	0.946	0.973	0.835	0.973	0.948	0.968	0.774
0.4	0.977	0.984	0.762	0.878	0.934	0.583	0.925	0.884	0.958	0.498
0.5	0.932	0.954	0.615	0.733	0.773	0.317	0.694	0.714	0.941	0.275
CRAYONS										
PSNR [dB]										
0.1	41.32	41.42	40.55	38.65	39.69	37.83	36.11	36.11	37.10	37.71
0.2	37.90	38.13	37.07	35.25	36.23	33.23	33.37	33.37	35.49	32.77
0.3	35.45	35.99	34.11	32.81	33.58	28.45	31.27	31.27	33.69	27.90
0.4	33.16	34.02	31.06	30.12	30.00	23.63	28.69	28.69	31.98	23.22
0.5	30.03	30.97	27.48	26.54	25.33	19.54	25.58	25.58	29.62	19.32
MAE										
0.1	0.40	0.40	1.10	0.51	0.46	0.52	0.79	0.79	1.23	0.54
0.2	0.83	0.82	1.65	1.06	0.93	1.17	1.45	1.45	1.65	1.27
0.3	1.30	1.27	2.39	1.74	1.50	2.26	2.25	2.25	2.16	2.54
0.4	1.87	1.79	3.53	2.71	2.37	4.52	3.39	3.39	2.74	5.15
0.5	2.75	2.58	5.60	4.46	4.28	9.01	5.34	5.34	3.58	10.17
SSIM										
0.1	0.991	0.991	0.981	0.983	0.987	0.982	0.979	0.979	0.964	0.978
0.2	0.980	0.981	0.961	0.962	0.972	0.946	0.955	0.955	0.951	0.936
0.3	0.967	0.969	0.928	0.931	0.951	0.851	0.920	0.920	0.934	0.832
0.4	0.948	0.954	0.865	0.875	0.906	0.666	0.858	0.858	0.914	0.645
0.5	0.904	0.918	0.742	0.760	0.785	0.436	0.742	0.742	0.884	0.433

TABLE VII
COMPARISON OF THE DENOISING EFFICIENCY OF THE PROPOSED NETWORK FOR IMPULSIVE NOISE REMOVAL WITH THE STATE-OF-THE-ART METHODS ON THE TEST DATASET [28].

ρ	IDCNN _{BSD500}	IDCNN _{GoogleV4}	DnCNN	FAPGF	FASTAMF	FFNRF	FRF	INRF	PARIGI	PGF
Average PSNR [dB]										
0.1	40.12	40.45	38.92	36.78	37.97	36.20	37.22	34.82	34.33	36.68
0.2	37.02	37.36	36.18	34.11	35.06	32.38	33.88	32.60	32.75	31.88
0.3	34.77	35.26	33.64	31.80	32.53	27.77	31.08	30.62	31.15	27.20
0.4	32.68	33.38	30.86	29.22	29.33	23.20	27.28	28.16	29.52	22.84
0.5	29.92	30.51	27.52	25.92	24.77	19.20	21.71	24.73	27.78	19.09
Average MAE										
0.1	0.46	0.45	1.18	0.72	0.60	0.72	0.59	1.01	1.62	0.63
0.2	0.92	0.90	1.71	1.31	1.12	1.34	1.21	1.65	2.18	1.40
0.3	1.42	1.39	2.41	2.02	1.72	2.44	2.01	2.45	2.82	2.75
0.4	2.01	1.94	3.49	3.04	2.60	4.78	3.30	3.59	3.58	5.50
0.5	2.86	2.75	5.45	4.80	4.59	9.48	6.56	5.66	4.53	10.75
Average SSIM										
0.1	0.989	0.989	0.980	0.977	0.983	0.975	0.981	0.974	0.949	0.976
0.2	0.978	0.979	0.962	0.955	0.967	0.940	0.961	0.949	0.931	0.929
0.3	0.963	0.966	0.932	0.920	0.944	0.841	0.935	0.913	0.908	0.815
0.4	0.944	0.949	0.872	0.856	0.898	0.645	0.875	0.848	0.881	0.624
0.5	0.904	0.911	0.748	0.736	0.771	0.414	0.666	0.718	0.845	0.420



(a) FRUITS



(b) BALLOONS



(c) PEPPERS



(d) CRAYONS

Fig. 13. Representative test images from benchmark dataset [28] for which numerical results were calculated.

IV. CONCLUSIONS

In this work, we introduced a switching filter that employs deep neural networks for impulsive noise removal in color images. The performed experiments revealed that the proposed network architecture which operates on a modified version of DnCNN network for impulse detection and adaptive mean filter for impulses restoration allows to efficiently remove impulses and outperforms state-of-the-art filters in terms of PSNR, MAE and SSIM measures. Future work will be focused on modification of the proposed neural network architecture

to detect and restore pixels contaminated by impulsive noise in a single stage network instead of using impulses detection and restoration as separate denoising operations.

ACKNOWLEDGMENT

This work was supported by the Polish National Science Centre under the project 2017/25/B/ST6/02219, and was also funded by the Statutory Research funds of Silesian University of Technology, Poland (Grant BK/200/Rau1/2019).

REFERENCES

- [1] R. Lukac, B. Smolka, K. Martin, K. Plataniotis, and A. Venetsanopoulos, "Vector filtering for color imaging," *IEEE Signal Processing Magazine*, vol. 22, no. 1, pp. 74–86, 2005.
- [2] C. Bonchelet, "Image noise models," in *Handbook of image and video processing*, ser. Communications, Networking and Multimedia, A. Bovik, Ed. Academic Press, 2005, pp. 397–410.
- [3] C. Liu, R. Szeliski, S. Bing Kang, C. L. Zitnick, and W. T. Freeman, "Automatic estimation and removal of noise from a single image," *IEEE Trans. on Pattern Analysis and Machine Intelligence*, vol. 30, no. 2, pp. 299–314, 2008.
- [4] B. Smolka, K. Malik, and D. Malik, "Adaptive rank weighted switching filter for impulsive noise removal in color images," *Journal of Real-Time Image Processing*, pp. 1–23, 2012.
- [5] L. Malinski and B. Smolka, "Self-tuning fast adaptive algorithm for impulsive noise suppression in color images," *Journal of Real-Time Image Processing*, 2019.
- [6] K. N. Plataniotis and A. N. Venetsanopoulos, "Color image filtering," in *Color Image Processing and Applications*, ser. Digital Signal Processing, Springer Berlin Heidelberg, 2000, pp. 51–105.
- [7] B. Smolka, K. Plataniotis, and A. Venetsanopoulos, *Nonlinear Signal and Image Processing: Theory, Methods, and Applications*, 2004, ch. Nonlinear Techniques for Color Image Processing, pp. 445–505.
- [8] M. Q. Phu, P. Tischer, and H. R. Wu, "Statistical analysis of impulse noise model for color image restoration," in *6th IEEE/ACIS International Conference on Computer and Information Science*, 2007, pp. 425–431.
- [9] R. Lukac, B. Smolka, K. N. Plataniotis, and A. N. Venetsanopoulos, "Entropy vector median filter," in *Pattern Recognition and Image Analysis*, 2003, pp. 1117–1125.

- [10] R. Lukac, B. Smolka, K. Martin, K. Plataniotis, and A. Venetsanopoulos, "Vector filtering for color imaging," *IEEE Signal Processing Magazine*, vol. 22, no. 1, pp. 74–86, 2005.
- [11] R. Lukac and K. Plataniotis, "A taxonomy of color image filtering and enhancement solutions," ser. *Advances in Imaging and Electron Physics*. Elsevier, 2006, vol. 140, pp. 187 – 264.
- [12] J. Astola, P. Haavisto, and Y. Neuvo, "Vector median filters," *Proceedings of the IEEE*, vol. 78, no. 4, pp. 678–689, 1990.
- [13] R. Lukac, B. Smolka, K. Plataniotis, and A. Venetsanopoulos, "Vector sigma filters for noise detection and removal in color images," *Journal of Visual Communication and Image Representation*, vol. 17, no. 1, pp. 1–26, 2006.
- [14] —, "Entropy vector median filter," *Lecture Notes in Computer Science*, vol. 2652, pp. 1117–1125, 2003.
- [15] R. Lukac, "Adaptive vector median filtering," *Pattern Recognition Letters*, vol. 24, no. 12, pp. 1889–1899, 2003.
- [16] M. E. Celebi, H. A. Kingravi, and Y. A. Aslandogan, "Nonlinear vector filtering for impulsive noise removal from color images," *Journal of Electronic Imaging*, vol. 16, no. 3, pp. 033 008–033 008–21, 2007.
- [17] B. Smolka and M. Perczak, "Generalized vector median filter," in *5th Inter. Symposium on Image and Signal Processing and Analysis*, 2007, pp. 254–257.
- [18] V. Chatzis and I. Pitas, "Fuzzy scalar and vector median filters based on fuzzy distances," *IEEE Trans. on Image Processing*, vol. 8, no. 5, pp. 731–734, 1999.
- [19] K. Plataniotis, D. Androustos, and A. Venetsanopoulos, "Adaptive fuzzy systems for multichannel signal processing," *Proceedings of the IEEE*, vol. 87, no. 9, pp. 1601–1622, 1999.
- [20] Y. Shen and K. Barner, "Fuzzy vector median-based surface smoothing," *IEEE Trans. on Visualization and Computer Graphics*, vol. 10, no. 3, pp. 252–265, 2004.
- [21] S. Morillas, V. Gregori, G. Peris-Fajarnés, and P. Latorre, "A new vector median filter based on fuzzy metrics," ser. *Lecture Notes in Computer Science*. Springer, 2005, vol. 3656, pp. 81–90.
- [22] J.-G. Camarena, V. Gregori, S. Morillas, and A. Sapena, "Fast detection and removal of impulsive noise using peer groups and fuzzy metrics," *Journal of Visual Communication and Image Representation*, vol. 19, no. 1, pp. 20 – 29, 2008.
- [23] S. Morillas, V. Gregori, and A. Hervás, "Fuzzy peer groups for reducing mixed Gaussian-impulse noise from color images," *IEEE Trans. on Image Processing*, vol. 18, no. 7, pp. 1452–1466, 2009.
- [24] L. Malinski and B. Smolka, "Fast adaptive switching technique of impulsive noise removal in color images," *Journal of Real-Time Image Processing*, 2016.
- [25] R. Garnett, T. Huegerich, C. Chui, and W. He, "A universal noise removal algorithm with an impulse detector," *IEEE Trans. on Image Processing*, vol. 14, no. 11, pp. 1747–1754, 2005.
- [26] Y. Deng, C. Kenney, M. Moore, and B. Manjunath, "Peer group filtering and perceptual color image quantization," in *Proc. of IEEE Intern. Symp. on Circuits and Systems*, vol. 4, 1999, pp. 21–24.
- [27] C. Kenney, Y. Deng, B. Manjunath, and G. Hewer, "Peer group image enhancement," *IEEE Trans. on Image Processing*, vol. 10, no. 2, pp. 326–334, 2001.
- [28] L. Malinski and B. Smolka, "Fast averaging peer group filter for the impulsive noise removal in color images," *Journal of Real-Time Image Processing*, no. 11, pp. 427–444, 2016.
- [29] L. Jin, H. Liu, X. Xu, and E. Song, "Quaternion-based color image filtering for impulsive noise suppression," *Journal of Electronic Imaging*, vol. 19, no. 4, p. 043003, 2010.
- [30] H. X. Geng Xin, "Quaternion based switching filter for impulse noise removal in color images," *Journal of Beijing University of Aeronautics And Astronautics*, no. 9, p. 1181, 2012.
- [31] G. Wang, Y. Liu, and T. Zhao, "A quaternion-based switching filter for colour image denoising," *Signal Processing*, vol. 102, pp. 216–225, 2014.
- [32] T.-C. Lin, "Decision-based filter based on svm and evidence theory for image noise removal," *Neural Computing and Applications*, vol. 21, no. 4, pp. 695–703, Jun 2012.
- [33] S. Liang, S. Lu, J. Chang, and C. Lin, "A novel two-stage impulse noise removal technique based on neural networks and fuzzy decision," *IEEE Trans. on Fuzzy Systems*, vol. 16, no. 4, pp. 863–873, 2008.
- [34] G. Kaliraj and S. Baskar, "An efficient approach for the removal of impulse noise from the corrupted image using neural network based impulse detector," *Image and Vision Computing*, vol. 28, no. 3, pp. 458 – 466, 2010.
- [35] M. S. Nair and V. Shankar, "Predictive-based adaptive switching median filter for impulse noise removal using neural network-based noise detector," *Signal, Image and Video Processing*, vol. 7, no. 6, pp. 1041–1070, Nov 2013.
- [36] I. Turkmen, "The ANN based detector to remove random-valued impulse noise in images," *Journal of Visual Communication and Image Representation*, vol. 34, pp. 28 – 36, 2016.
- [37] S. Lefkimmiatis, "Non-local color image denoising with convolutional neural networks," in *2017 IEEE Conference on Computer Vision and Pattern Recognition (CVPR)*, 2017, pp. 5882–5891.
- [38] —, "Universal denoising networks : A novel CNN architecture for image denoising," in *2018 IEEE/CVF Conference on Computer Vision and Pattern Recognition*, 2018, pp. 3204–3213.
- [39] K. Zhang, W. Zuo, and L. Zhang, "Ffdnet: Toward a fast and flexible solution for CNN-based image denoising," *IEEE Trans. on Image Processing*, vol. 27, no. 9, pp. 4608–4622, 2018.
- [40] B. Fu, X. Zhao, Y. Li, X. Wang, and Y. Ren, "A convolutional neural networks denoising approach for salt and pepper noise," *Multimedia Tools and Applications*, 2018.
- [41] Y. Amaria, T. Miyazakia, Y. Koshimuraa, Y. Yokoyamaa, and H. Yamamoto, "A study on impulse noise reduction using cnn learned by divided images," in *6th IIAE International Conference on Industrial Application Engineering*, 2018, pp. 93–100.
- [42] K. Radlak, L. Malinski, and B. Smolka, "Deep learning for impulsive noise removal in color digital images," vol. 10996, 2019.
- [43] K. Zhang, W. Zuo, Y. Chen, D. Meng, and L. Zhang, "Beyond a Gaussian denoiser: Residual learning of deep CNN for image denoising," *IEEE Trans. on Image Processing*, vol. 26, no. 7, pp. 3142–3155, 2017.
- [44] W. Zuo, K. Zhang, and L. Zhang, *Convolutional Neural Networks for Image Denoising and Restoration*. Springer International Publishing, 2018, pp. 93–123.
- [45] K. Simonyan and A. Zisserman, "Very deep convolutional networks for large-scale image recognition," in *International Conference on Learning Representations*, 2015.
- [46] A. Krizhevsky, I. Sutskever, and G. E. Hinton, "Imagenet classification with deep convolutional neural networks," in *Advances in Neural Information Processing Systems* 25, 2012, pp. 1097–1105.
- [47] S. Ioffe and C. Szegedy, "Batch normalization: Accelerating deep network training by reducing internal covariate shift," in *Proceedings of the 32Nd International Conference on International Conference on Machine Learning - Volume 37*, ser. ICML'15, 2015, pp. 448–456.
- [48] K. He, X. Zhang, S. Ren, and J. Sun, "Deep residual learning for image recognition," in *2016 IEEE Conference on Computer Vision and Pattern Recognition (CVPR)*, 2016, pp. 770–778.
- [49] K. Zhang, W. Zuo, S. Gu, and L. Zhang, "Learning deep cnn denoiser prior for image restoration," in *2017 IEEE Conference on Computer Vision and Pattern Recognition (CVPR)*, 2017, pp. 2808–2817.
- [50] X. Glorot and Y. Bengio, "Understanding the difficulty of training deep feedforward neural networks," in *Proceedings of the Thirteenth International Conference on Artificial Intelligence and Statistics*, ser. *Proceedings of Machine Learning Research*, Y. W. Teh and M. Titterton, Eds., vol. 9, 2010, pp. 249–256.
- [51] D. Kingma and L. Ba, "Adam: A method for stochastic optimization," in *International Conference on Learning Representations*, 2015.
- [52] P. Arbelaez, M. Maire, C. Fowlkes, and J. Malik, "Contour detection and hierarchical image segmentation," *IEEE Trans. Pattern Anal. Mach. Intell.*, vol. 33, no. 5, pp. 898–916, 2011.
- [53] M. Everingham, L. Van Gool, C. K. I. Williams, J. Winn, and A. Zisserman, "The PASCAL Visual Object Classes Challenge 2007 (VOC2007) Results," <http://www.pascal-network.org/challenges/VOC/voc2007/workshop/index.html>.
- [54] A. Kuznetsova, H. Rom, N. Alldrin, J. Uijlings, I. Krasin, J. Pont-Tuset, S. Kamali, S. Popov, M. Mallocci, T. Duerig, and V. Ferrari, "The open images dataset v4: Unified image classification, object detection, and visual relationship detection at scale," *arXiv:1811.00982*, 2018.
- [55] Zhou Wang, A. C. Bovik, H. R. Sheikh, and E. P. Simoncelli, "Image quality assessment: from error visibility to structural similarity," *IEEE Trans. on Image Processing*, vol. 13, no. 4, pp. 600–612, 2004.
- [56] J.-G. Camarena, V. Gregori, S. Morillas, and A. Sapena, "Two-step fuzzy logic-based method for impulse noise detection in colour images," *Pattern Recognition Letters*, vol. 31, no. 13, pp. 1842 – 1849, 2010.
- [57] S. Schulte, S. Morillas, V. Gregori, and E. E. Kerre, "A new fuzzy color correlated impulse noise reduction method," *IEEE Trans. on Image Processing*, vol. 16, no. 10, pp. 2565–2575, Oct 2007.
- [58] J. Delon and A. Desolneux, "A patch-based approach for removing impulse or mixed Gaussian-impulse noise," *SIAM Journal on Imaging Sciences*, vol. 6, no. 2, pp. 1140–1174, 2013.

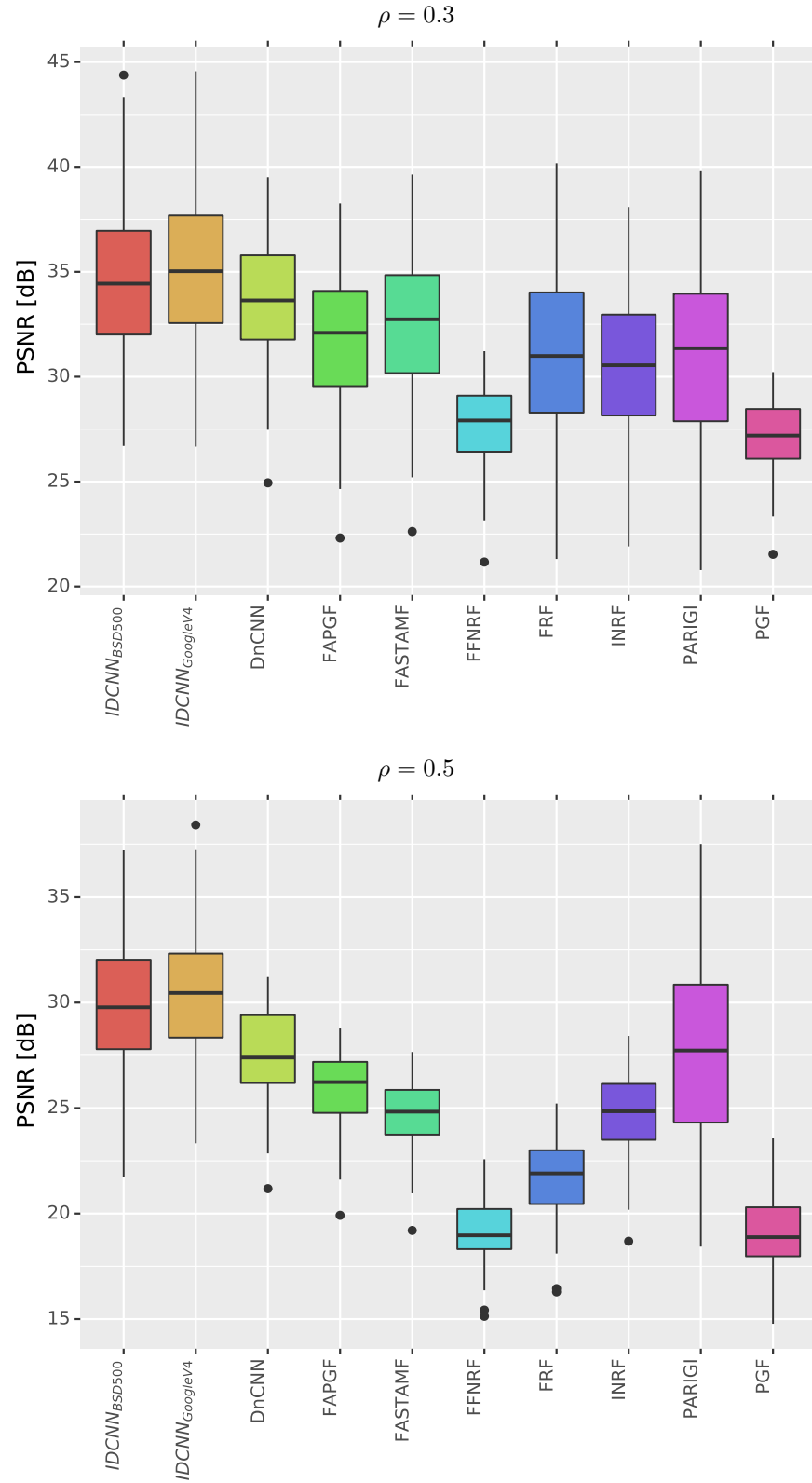


Fig. 14. The representative boxplots that shows the distribution of the obtained results for the analyzed methods on the test dataset [28].

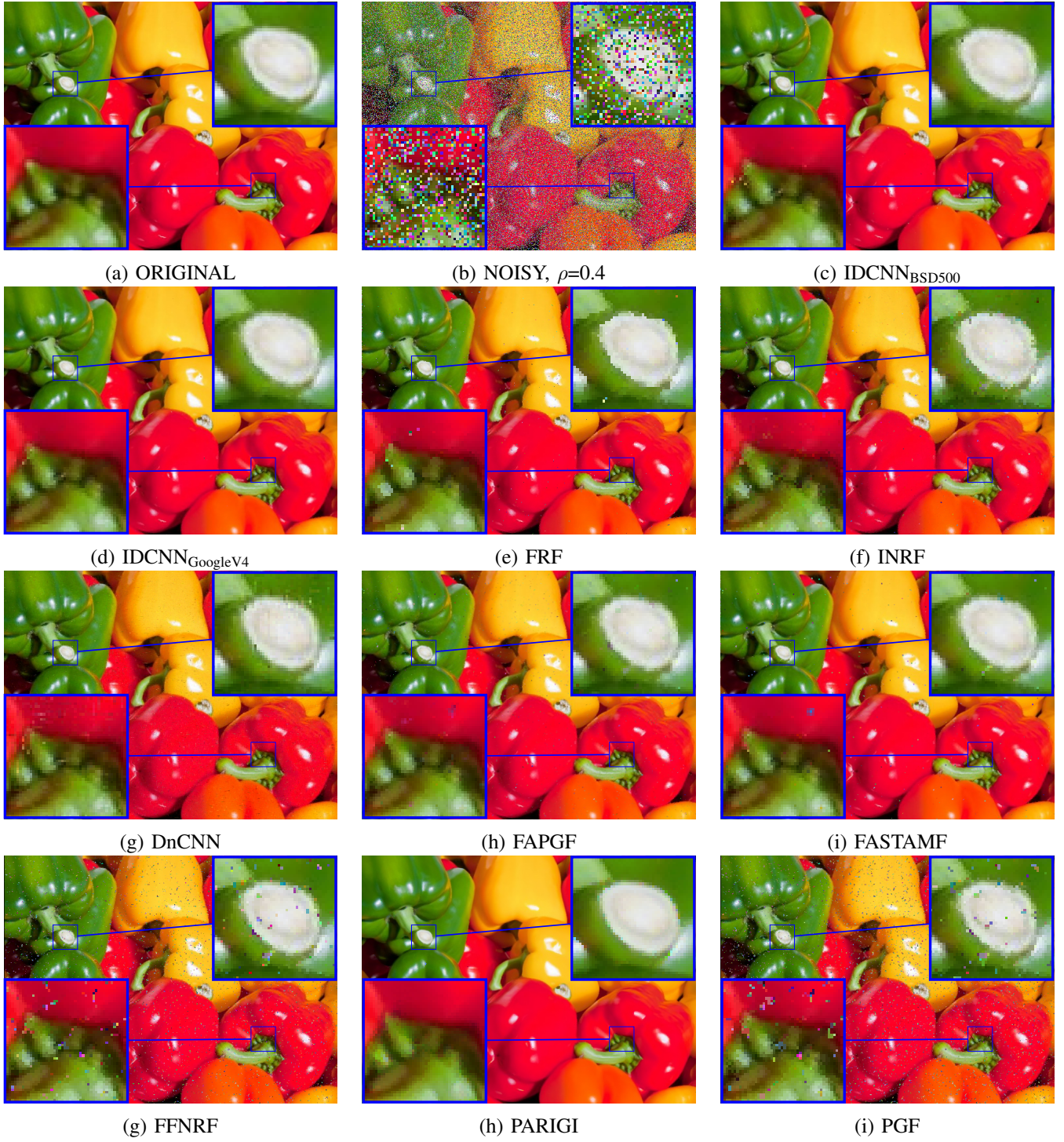
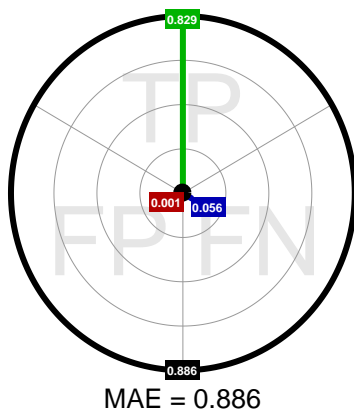
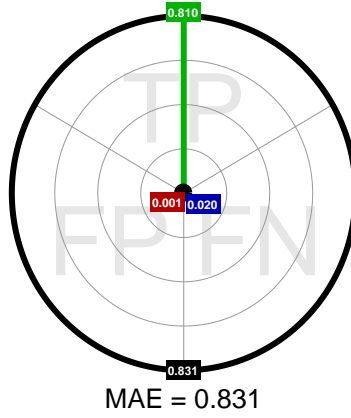
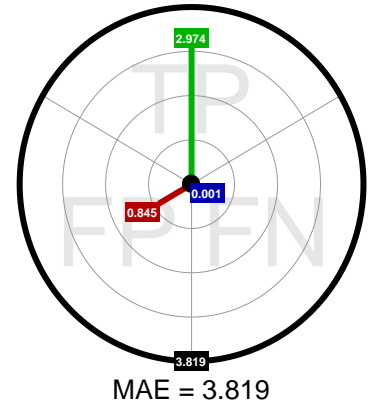
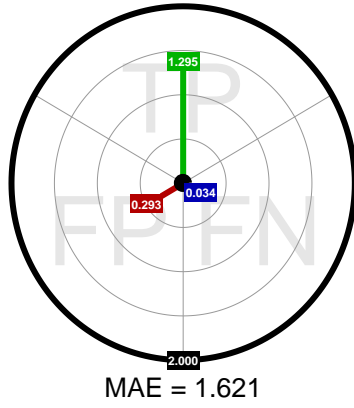


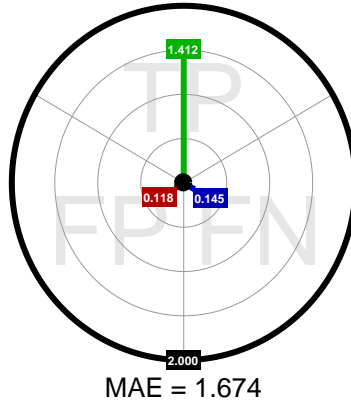
Fig. 15. Visual comparison of the filtering efficiency using a part of the PEPPERS image ($\rho = 0.4$).

(a) IDCNN_{BSD500}(b) IDCNN_{GoogleV4}

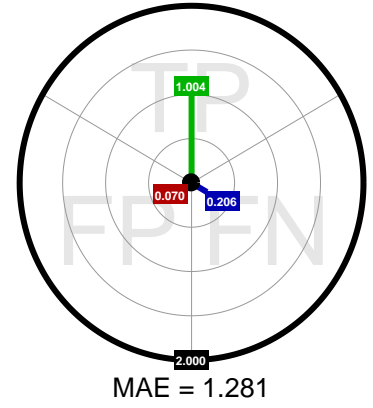
(c) DnCNN



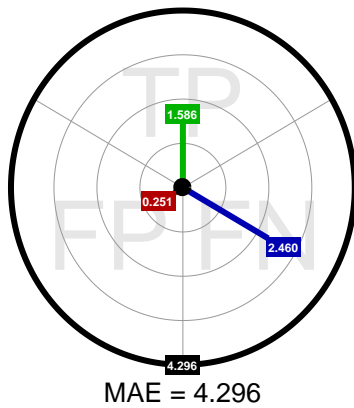
(g) FRF



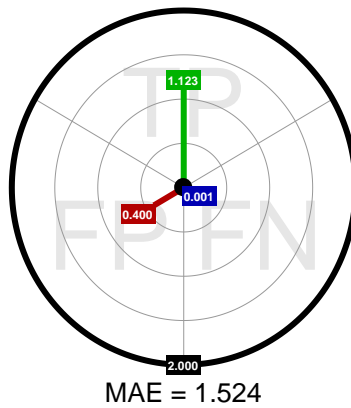
(h) FAPGF



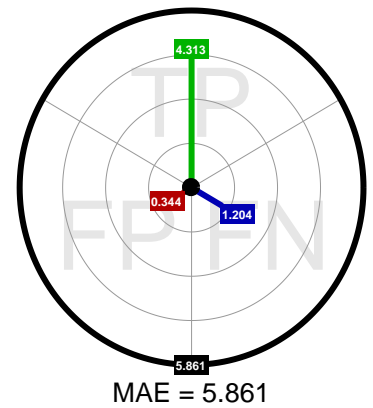
(i) FASTAMF



(g) FFNRF



(h) PARIGI



(i) PGF

Fig. 16. The diagrams that show what portion of the MAE error was caused by the improper decision of the used filter from classification perspective. These diagrams were obtained for the PEPPERS image ($\rho = 0.4$). The main contribution to the total error is made by the replacement (interpolation) of the correctly detected impulses.